Direct Detection of Dimer Orbitals in $Ba_5AlIr_2O_{11}$

Y. Wang,[1,*] Ruitang Wang,[2,3,7] Jungho Kim,[4] M. H. Upton,[4] D. Casa,[4] T. Gog,[4] G. Cao,[5] G. Kotliar,[1,6] M. P. M. Dean,[1,†] and X. Liu[2,‡]

[1]*Department of Condensed Matter Physics and Materials Science, Brookhaven National Laboratory, Upton, New York 11973, USA*

[2]*School of Physical Science and Technology, ShanghaiTech University, Shanghai 201210, China*

[3]*Beijing National Laboratory for Condensed Matter Physics and Institute of Physics, Chinese Academy of Sciences, Beijing 100190, China*

[4]*Advanced Photon Source, Argonne National Laboratory, Argonne, Illinois 60439, USA*

[5]*Department of Physics, University of Colorado Boulder, Boulder, Colorado 80309, USA*

[6]*Physics and Astronomy Department, Rutgers University, Piscataway, New Jersey 08854, USA*

[7]*School of Physical Sciences, University of Chinese Academy of Sciences, Beijing 100049, China*

(Received 12 October 2018; published 11 March 2019)

The electronic states of many Mott insulators, including iridates, are often conceptualized in terms of localized atomic states such as the famous "$J_{\mathrm{eff}} = 1/2$ state." Although orbital hybridization can strongly modify such states and dramatically change the electronic properties of materials, probing this process is highly challenging. In this Letter, we directly detect and quantify the formation of dimer orbitals in an iridate material $Ba_5AlIr_2O_{11}$ using resonant inelastic x-ray scattering. Sharp peaks corresponding to the excitations of dimer orbitals are observed and analyzed by a combination of density functional theory calculations and theoretical simulations based on an Ir-Ir cluster model. Such partially delocalized dimer states lead to a redefinition of the angular momentum of the electrons and changes in the magnetic and electronic behaviors of the material. We use this to explain the reduction of the observed magnetic moment with respect to predictions based on atomic states. This study opens new directions to study dimerization in a large family of materials, including solids, heterostructures, molecules, and transient states.

DOI: 10.1103/PhysRevLett.122.106401

Many of the most interesting phases in correlated quantum materials occur in systems with strong Coulomb repulsion U, which tends to drive electron localization via the Mott insulating mechanism [1]. Because of this, we often conceptualize the electronic and magnetic properties of these systems in terms of localized states [2], even though many of the most interesting cases occur when there is strong competition between U and electron hopping t. Of particular interest in this regard is the localized $J_{\mathrm{eff}} = 1/2$ state [3], which is the conceptual building block for a host of fascinating proposed and observed states, including frustrated magnets [4–10], topological insulators [11,12], and possibly even unconventional superconductors [13]. Hopping between IrO_6 octahedra delocalizes the electrons and is expected to be relevant in many classes of iridate (or other heavy d-electron materials) with edge- or face-sharing octahedra [14–19]. This can heavily modify, or even destroy, the $J_{\mathrm{eff}} = 1/2$ state, motivating arguments about how best to conceptualize the electronic state of iridates [14,20,21]. Directly probing these states is therefore highly desirable. In the simplest case of dimerization between neighboring pairs of IrO_6 octahedra, one expects the formation of quasilocalized dimer orbitals, which are difficult to probe by photoemission due to the absence of dispersive bands and hard to probe optically as dipole optical selection rules means that transitions within a orbital manifold are nominally forbidden. Resonant inelastic x-ray scattering (RIXS), on the other hand, has been shown as a particularly incisive probe of on-site localized transitions in the iridates, but, as far as we are aware, has never definitively isolated an excitation associated with dimerization [22,23].

In this Letter, we establish that RIXS can directly measure peaks associated with orbital dimerization and that a quantitative description of the dimer electronic configuration can be extracted using density functional theory (DFT) calculations and multiplet modeling. For this study we employ face-sharing iridiate $Ba_5AlIr_2O_{11}$ and account for how these interactions modify the $J_{\mathrm{eff}} = 1/2$ state expected on the nominally $5d^5$ atom in this crystal, reproducing the previously measured reduction in the magnetic moment [24]. We argue that, given the proven ability of RIXS to measure molecules, oxide heterostructures, and even ultrafast transient states, this has great potential to probe orbital dimerization under many different circumstances [25–31].

Single crystal samples of $Ba_5AlIr_2O_{11}$ were synthesized using the self-flux method as described in Refs. [24,32]. Previous diffraction and transport measurements confirm high sample quality [24]. $Ba_5AlIr_2O_{11}$ forms an orthorhombic unit cell with space group *Pnma* (No. 62) with

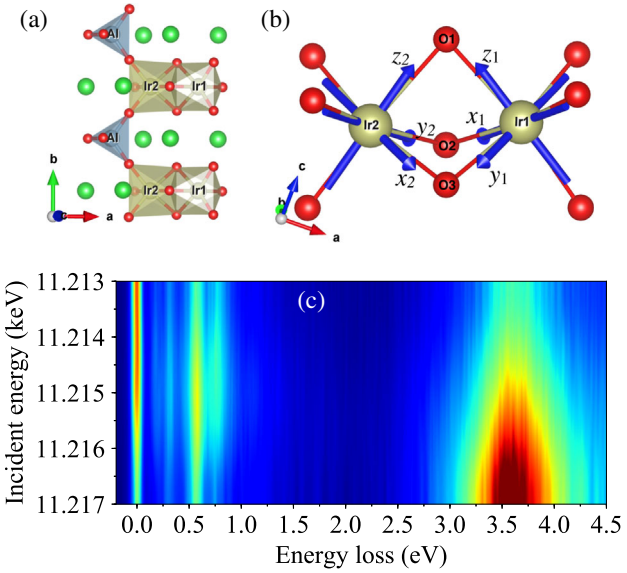

FIG. 1. (a) Crystal structure of $Ba_5AlIr_2O_{11}$. The two inequivalent IrO_6 octahedra are labeled Ir1 and Ir2 and colored in dark yellow. Quasi-one-dimensional Ir chain structures occur via the connection of these octahedra through AlO_4 tetrahedra along the b axis. (b) Illustration of the local Cartesian coordinates used in the definition of t_{2g} orbitals. The orientation of the local coordinates is chosen such that the x, y, z axes are all at an equal angle [$\arccos(1/\sqrt{3})$ rad] with respect to the Ir1—Ir2 bond and the z axis lies in the Ir1-O1-Ir2 plane. The x, y, z axes lie approximately along the Ir—O bonds in this setting. (c) RIXS map showing the intra-t_{2g} and $t_{2g} \rightarrow e_g$ excitations.

$a = 18.76$, $b = 5.755$, and $c = 11.06$ Å [24]. As shown in Fig. 1(a), two face-sharing IrO_6 octahedra form isolated dimers, which are then connected by AlO_4 tetrahedra. These two inequivalently coordinated face-sharing Ir octahedra in a dimer are labeled as Ir1 and Ir2, as shown in Figs. 1(a) and 1(b). RIXS experiments were performed at the Ir-L_3 edge by using the MERIX instrument at sector 27 of the Advanced Photon Source [33]. A 2 m Si (884) diced analyzer was used to energy resolve the scattered x rays. Different incident beam monochromation setups were tested before settling with a combined ~80 meV total resolution (full width at half maximum). Data were collected with a horizontal scattering geometry with the incident x-ray polarization parallel to the scattering plane (π channel). The sample was mounted such that the [010] Ir chain direction and the [101] sample surface normal are in the scattering plane. Data were collected using an incident x-ray angle α close to 26° and a detector angle 2θ close to 90° unless otherwise specified.

We initially surveyed incident-energy-dependent RIXS at room temperature as shown in Fig. 1(c). The low-energy excitations below 1.2 eV resonate at 11.215 keV and can be assigned to intra-t_{2g} transitions by comparison to previous work; $t_{2g} \rightarrow e_g$ transitions occur around 3.6 eV and resonate at higher incident energies [22,34,35]. A more detailed incident energy dependence was mapped at 40 K with 80 meV energy resolution [36], focusing on the low-energy intra-t_{2g} excitations. The spectrum is plotted in Figs. 2(a) and 2(b), where five distinct peaks can be clearly identified. They are labeled A–E with energies 0.18, 0.32, 0.565, 0.74, and 1.13 eV, respectively. These features show no appreciable dispersive behavior in their peak energies [see Fig. 2(c)] at various momentum transfer $\boldsymbol{Q}$ over almost one Brillouin zone in the chain direction, suggesting that the excitations are confined within a dimer and that coupling through the AlO_4 tetrahedra can be neglected on these energy scales. We note that pure spin flip excitations are not observed here, almost certainly because they occur on a too low energy scale.

We use a two-site cluster model for Ir1 and Ir2 [see Fig. 1(b)] to simulate the measured RIXS spectrum. The t_{2g} orbitals of Ir1 and Ir2 are defined with respect to the local Cartesian coordinates shown in Fig. 1(b). The EDRIXS [37] toolkit developed in the COMSCOPE project [38,39] is used to diagonalize the Hamiltonian and simulate the RIXS

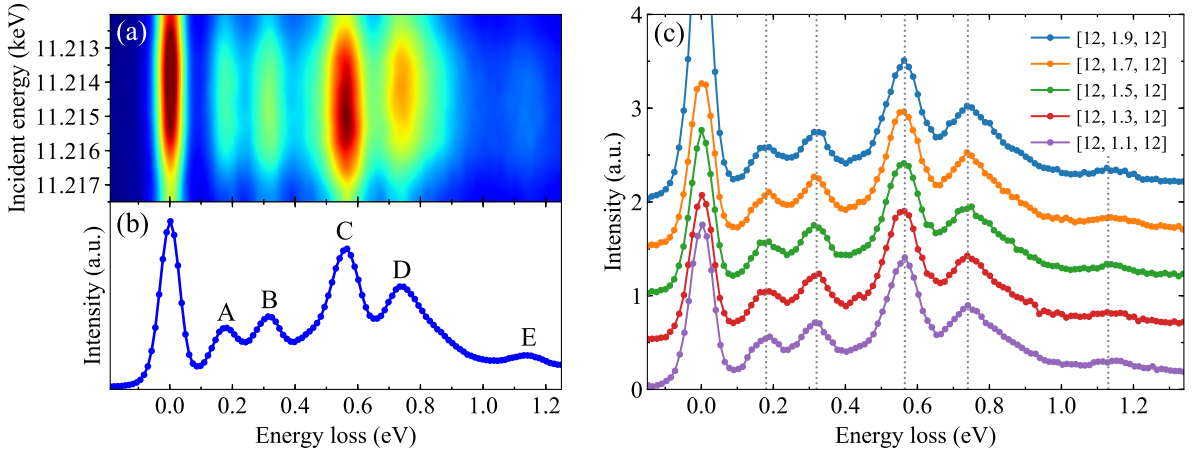

FIG. 2. (a) High-resolution RIXS map at 40 K. (b) The excitation spectrum integrated over ±2 eV with respect to the resonant energy of 11.215 keV. (c) Orbital excitations of $Ba_5AlIr_2O_{11}$ show no significant $\boldsymbol{Q}$ dependence indicative of localized states.

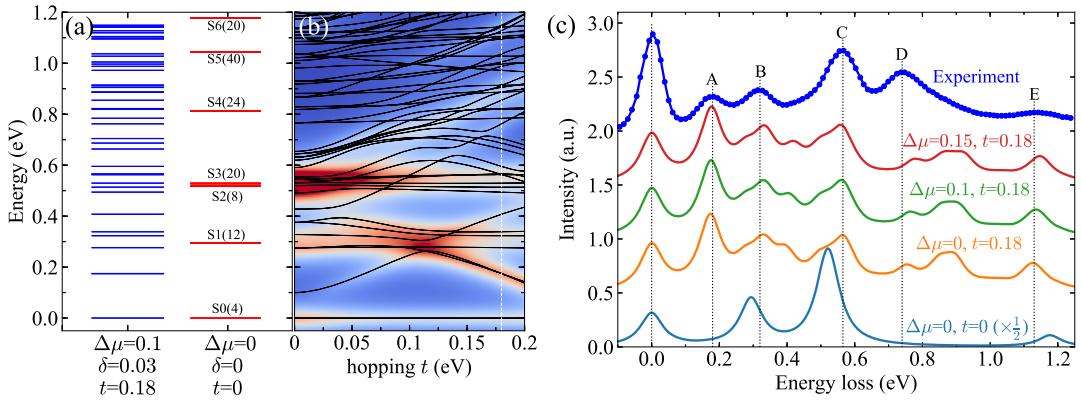

FIG. 3. (a) Illustration of the splitting of the trivial DPS after turning on hopping t. The letter S is used to label these DPSs and the numbers in parentheses are their degeneracy. (b) The solid lines are the energy spectrum of the Ir-Ir cluster model as a function of hopping t at $\Delta\mu = 0.1$ eV, $\delta = 0.03$ eV, and the color map indicates the corresponding simulated RIXS intensity. The vertical dotted line indicates $t = 0.18$ eV. (c) The simulated RIXS spectrum at several chosen parameters are compared with the experimental result; $\delta = 0$ for the bottom light blue curve and $\delta = 0.03$ for all others.

spectrum, with the real experimental geometry and polarization applied. The energy resolution is set to be 80 meV full width at half maximum. More details of the RIXS simulation can be found in the Supplemental Material [40].

To understand the electronic structure that gives rise to the observed excitations, we start with the nonphysical condition where the Ir1-Ir2 hopping and the noncubic crystal field (CF) are set to zero. With the octahedra decoupled, the electronic structure is determined by the spin-orbit coupling (SOC) λ, the on-site Coulomb U, and Hund's J_H interactions. We use a t_{2g} Kanamori-type Hamiltonian to treat U and J_H, which can be written as

$$\hat{H}_U = U\sum_{\alpha}\hat{n}_{\alpha\uparrow}\hat{n}_{\alpha\downarrow} + U'\sum_{\alpha\neq\beta}\hat{n}_{\alpha\uparrow}\hat{n}_{\beta\downarrow} + U''\sum_{\alpha<\beta,\sigma}\hat{n}_{\alpha\sigma}\hat{n}_{\beta\sigma} - J_H\sum_{\alpha\neq\beta}\hat{d}^{\dagger}_{\alpha\uparrow}\hat{d}_{\alpha\downarrow}\hat{d}^{\dagger}_{\beta\downarrow}\hat{d}_{\beta\uparrow} + J_H\sum_{\alpha\neq\beta}\hat{d}^{\dagger}_{\alpha\uparrow}\hat{d}^{\dagger}_{\alpha\downarrow}\hat{d}_{\beta\downarrow}\hat{d}_{\beta\uparrow}, \quad (1)$$

where $\alpha(\beta) = d_{zx}, d_{zy}, d_{xy}$ is the t_{2g} orbital index. $\sigma = \uparrow, \downarrow$ is the spin index. $U' = U - 2J_H$ and $U'' = U - 3J_H$. U is chosen to be 2 eV through all the calculations [46]. With hopping forbidden, the electrons are localized to form $|d^4\rangle$ on Ir1 and $|d^5\rangle$ on Ir2, with atomic states $|d^4, J_{\text{eff}} = 0, 1, 2, 2'\rangle$ and $|d^5, J_{\text{eff}} = 1/2, 3/2\rangle$, respectively. States $J_{\text{eff}} = 2$ and $J_{\text{eff}} = 2'$ both have total angular momentum 2, but are of different energies. Excitations can happen within each atomic state set, and their energies are determined by Hund's coupling and SOC. With $J_H = 0.3$ eV and $\lambda = 0.345$ eV, which are consistent with earlier work [47–49], the simulated RIXS spectrum is shown as the light blue curve in Fig. 3(c), where three peaks are found. The peak near B comes from the excitations from $|d^4, J_{\text{eff}} = 0\rangle$ to $|d^4, J_{\text{eff}} = 1\rangle$ states. The peak near C contains two excitations with very close energies, one is from $|d^5, J_{\text{eff}} = 1/2\rangle$ to $|d^5, J_{\text{eff}} = 3/2\rangle$ states and another is from $|d^4, J_{\text{eff}} = 0\rangle$ to $|d^4, J_{\text{eff}} = 2\rangle$ states. Peak E is determined by the excitations from $|d^4, J_{\text{eff}} = 0\rangle$ to $|d^4, J_{\text{eff}} = 2'\rangle$. Obviously, our experimental observations have far richer features than this simulated RIXS spectrum at the isolated atom level. The activation of the intersite hopping will strongly mix the $|d^4; d^5\rangle$ and $|d^5; d^4\rangle$ configurations, which will not only tune the energy of the excitations but also create new delocalized states and excitation channels. Here, we use $|d^{n_1}; d^{n_2}\rangle$ to represent a direct product state (DPS) of the dimer, where Ir1 has n_1 electrons and Ir2 has n_2 electrons.

To estimate the hopping and the noncubic crystal field, we performed a first-principles DFT calculation using Vienna *ab initio* Simulation Package (VASP) [41–43,50] and fit a t_{2g} tight-binding Hamiltonian to the result using the maximally localized Wannier functions method [51,52]. We set $\lambda = U = J_H = 0$, as they are included explicitly in our model later. For simplicity, we assume a trigonal local CF for the IrO_6 octahedra in $Ba_5AlIr_2O_{11}$. Under this approximation, the Hamiltonian $\hat{V}^{12}$ for the hopping between Ir1 and Ir2 takes a simple form in the t_{2g} basis,

$$\hat{V}^{12} = \begin{array}{c} \\ d_{z_1x_1} \\ d_{z_1y_1} \\ d_{x_1y_1} \end{array} \begin{array}{c} \begin{array}{ccc} d_{z_2x_2} & d_{z_2y_2} & d_{x_2y_2} \end{array} \\ \begin{pmatrix} -t & t' & -t \\ t' & -t & -t \\ -t & -t & t' \end{pmatrix} \end{array} + \text{H.c.}, \quad (2)$$

where t and t' are the hopping parameters. Our DFT calculation gives $t = 0.18$ eV, and $t' \approx 0.2t$. The on-site trigonal CF Hamiltonian is

$$\hat{H}^{1(2)}_{\text{CF}} = \begin{pmatrix} \mu_{1(2)} & -\delta & -\delta \\ -\delta & \mu_{1(2)} & -\delta \\ -\delta & -\delta & \mu_{1(2)} \end{pmatrix}, \quad (3)$$

where μ_1 and μ_2 are the chemical potentials for Ir1 and Ir2, respectively. Their difference $\Delta\mu = \mu_1 - \mu_2$ is about 0.1 eV. This chemical potential difference distinguishes the two inequivalent IrO_6 octahedra [24,53] and induces partial charge disproportionation in $Ba_5AlIr_2O_{11}$. δ is estimated to be 0.03 eV from the DFT calculation. The two-site Ir1-Ir2 cluster Hamiltonian is diagonalized in the subspace with nine electrons in total to get the energy spectrum.

For the isolated Ir1 and Ir2 condition discussed earlier, the energy levels (0–1.2 eV) of these DPSs at $\Delta\mu = 0$, $\delta = 0$, and $t = 0$ are shown as the red plateaus and labeled by S in Fig. 3(a). After turning on the hopping t, dimer orbitals will form by superposition of the atomic orbitals of Ir1 and Ir2. As a result, the configurations $|d^4; d^5\rangle$ and $|d^5; d^4\rangle$ will mix with each other. With the DFT derived $\{t, t', \Delta\mu, \delta\}$, and the local interaction $J_H = 0.3$ eV and $\lambda = 0.345$ eV, the calculated energy levels of these delocalized dimer states are shown as blue lines in Fig. 3(a). As can be seen in Fig. 3(c), the calculated RIXS spectrum with these parameters agrees quite well with our experimental observations. Peaks A and D, which were missing in the localized picture, now appear in the simulated RIXS spectrum as excitations between delocalized dimerized states. For example, peak A is from the excitation from the ground state to the first excited state. The weights of $|d^4; d^5\rangle$ and $|d^5; d^4\rangle$ configurations are, respectively, 0.608 and 0.392 in the ground state and 0.560 and 0.440 in the first excited state.

To further appreciate the competition between the atomic SOC λ, Hund's coupling J_H, and the delocalization hopping t, the evolution of the energy spectrum of these dimer states as a function of hopping t is presented in Fig. 3(b). In this calculation, other parameters except hopping t are fixed. In Fig. 3(b), the solid lines are the relative energies of the dimer states, and the underlying color map represents the calculated corresponding RIXS intensities. We can see that each level S splits into many dimer states and the energy splitting increases with increasing t. In the small t regime, local on-site J_H and λ dominate the Hamiltonian, so the mixing mainly occurs within the same level S and the energy splitting is not far away from the center of each level S. When increasing t, it will compete with J_H and λ to induce more mixing between different levels S, which are reflected as the crossing of energy levels in Fig. 3(b). For example, the energy of the first excited state split from the level $S0$ increases at small t regime to a maximum and then decreases at $t \gtrsim 0.12$. Another state split from level $S1$ is pushed down to cross with it and has very similar energy.

Besides peaks A–E, the calculated RIXS intensity also shows some shoulders around the main peaks that are not resolved in the experimental RIXS spectrum. They might be washed out by longer range hopping or itineracy not captured in the cluster model. We also find that the energy of the dimer states and the RIXS spectrum are not sensitive to $\Delta\mu$ in the region $\Delta\mu < t$ [see Fig. 3(c)], because t dominates the energy spectrum in this region and the energy splitting of the bonding and antibonding orbitals is as large as $2.5t$. More details on the competition between $\Delta\mu$ and the hopping t with different energy strengths are shown in the Supplemental Material [40]. At $\Delta\mu = 0.1$ eV and $t = 0.18$ eV, the calculated charge disproportionation between Ir1 and Ir2 is about 0.218 electrons, which is close to 0.3 electrons reported in previous DFT calculation [53].

Combining RIXS measurements and DFT calculations, we show that the electronic structure of $Ba_5AlIr_2O_{11}$ needs to be described by partially delocalized dimer orbitals, rather than $J_{\text{eff}} = 1/2$ atomic states in the strong SOC limit. It is interesting to notice that dimer orbitals can still occur in $Ba_5AlIr_2O_{11}$ even if U is large, as due to the noninteger average Ir valence of 4.5, the Mott mechanism cannot stop hopping between the Ir sites. The dimerization process significantly changes the magnetic properties of $Ba_5AlIr_2O_{11}$. The calculated effective local moment per dimer is about $1\,\mu_B$ in $Ba_5AlIr_2O_{11}$, which is consistent with the experimental results [24], but is much smaller than the value $1.732\,\mu_B$ expected for two isolated Ir sites: a $J_{\text{eff}} = 1/2$ on Ir2 and a $J_{\text{eff}} = 0$ singlet on Ir1. It indicates that the symmetry of the magnetic order parameter has deviated from the ideal spherical symmetry. Indeed, unlike $3d$ magnetic Mott insulators, where the order parameter can be described by pure local physics, it is common that the order parameter cannot be well described by a pure local object in many iridates due to the extended orbitals and much stronger intersite hoppings. For instance, reduced effective local moments have been observed in many d^5 iridates, such as Sr_2IrO_4 [54,55], $Sr_3Ir_2O_7$ [56], and pyrochlore iridates [57–59]. Another interesting case is the exotic magnetic moments found in some d^4 iridates [60], where the local ground state is a nonmagnetic singlet. This peculiar behavior is found to be caused by the virtual intersite exchange process [61], so a local single atomic description is not appropriate here either. We also emphasize that the cluster model used in this Letter can be straightforwardly applied to simulate the RIXS spectrum of the 6H-hexagonal oxides $Ba_3AB_2O_9$ (A = In, Y, Lu, Na and B = Ru, Ir) [16,62,63] and similar dimer excitations can be expected in these compounds. This theoretical method can also be generalized to study other systems with strong nonlocal electronic itinerancy, such as the pyrochlore iridates, where possible low-energy dimer excitations (around 0.1 eV) have been observed in the RIXS spectrum [64–67].

In summary, we find new peaks corresponding to the excitations of dimer orbitals in the experimental RIXS spectrum of $Ba_5AlIr_2O_{11}$. The DFT calculations and the RIXS simulations confirm that the hopping strength between Ir1 and Ir2 in $Ba_5AlIr_2O_{11}$ is indeed strong enough to form dimer orbitals, and their excitations explain the observed features in the measured RIXS spectrum. Furthermore, our analysis well explained the observed

reduction of the magnetic moment. This Letter establishes RIXS as a spectroscopy tool to probe the formation of delocalized dimer orbitals and characterize their microscopic properties, which may open new directions to study delocalization in other dimerized strongly correlated materials by RIXS with widespread potential applications in molecules, oxide heterostructures, and even ultrafast transient states.

We thank John Hill, Sergey Streltsov, Hu Miao and Keith Gilmore for discussions and support related to this project. Work at ShanghaiTech University was supported by the ShanghaiTech University startup fund and partially supported by MOST of China under Grant No. 2016YFA0401000 (experiment, data analysis and leading writing). R. W. was supported by the international partnership program of Chinese Academy of Sciences under Grant No. 112111KYSB20170059 (experiment and data analysis). Work at Brookhaven National Laboratory was supported by the U.S. Department of Energy, Office of Science, Basic Energy Sciences as a part of the Computational Materials Science Program through the Center for Computational Design of Functional Strongly Correlated Materials and Theoretical Spectroscopy (calculations, software development and data interpretation), Office of Basic Energy Sciences, Early Career Award Program under Award No. 1047478 (writing) and the U.S. Department of Energy, Office of Science, Office of Basic Energy Sciences, under Award No. DE-SC0012704. Work at Argonne National Laboratory was supported by the U.S. Department of Energy, Office of Science, under Award No. DE-AC-02-06CH11357 (synchrotron user facility instrumentation). Work at the University of Colorado, Boulder, was funded via NSF Grant No. DMR-1712101 (materials synthesis).

Note added in the proof.—Recently, dimer excitations were also reported in $Ba_3CeIr_2O_9$ [68].

*yilinwang@bnl.gov
†mdean@bnl.gov
‡liuxr@shanghaitech.edu.cn

[1] B. Keimer and J. E. Moore, The physics of quantum materials, Nat. Phys. **13**, 1045 (2017).
[2] D. I. Khomskii, *Transition Metal Compounds* (Cambridge University Press, Cambridge, England, 2014).
[3] G. Chen and L. Balents, Spin-orbit effects in $Na_4Ir_3O_8$: A hyper-kagome lattice antiferromagnet, Phys. Rev. B **78**, 094403 (2008).
[4] J. Chaloupka, G. Jackeli, and G. Khaliullin, Kitaev-Heisenberg Model on a Honeycomb Lattice: Possible Exotic Phases in Iridium Oxides A_2IrO_3, Phys. Rev. Lett. **105**, 027204 (2010).
[5] Y. Okamoto, M. Nohara, H. Aruga-Katori, and H. Takagi, Spin-Liquid State in the $S = 1/2$ Hyperkagome Antiferromagnet $Na_4Ir_3O_8$, Phys. Rev. Lett. **99**, 137207 (2007).
[6] L. Balents, Spin liquids in frustrated magnets, Nature (London) **464**, 199 (2010).
[7] M. J. Lawler, A. Paramekanti, Y. B. Kim, and L. Balents, Gapless Spin Liquids on the Three-Dimensional Hyperkagome Lattice of $Na_4Ir_3O_8$, Phys. Rev. Lett. **101**, 197202 (2008).
[8] Y. Zhou, P. A. Lee, T.-K. Ng, and F.-C. Zhang, $Na_4Ir_3O_8$ as a 3D Spin Liquid with Fermionic Spinons, Phys. Rev. Lett. **101**, 197201 (2008).
[9] G. Chen, R. Pereira, and L. Balents, Exotic phases induced by strong spin-orbit coupling in ordered double perovskites, Phys. Rev. B **82**, 174440 (2010).
[10] G. Chen and L. Balents, Spin-orbit coupling in d^2 ordered double perovskites, Phys. Rev. B **84**, 094420 (2011).
[11] D. Pesin and L. Balents, Mott physics and band topology in materials with strong spin–orbit interaction, Nat. Phys. **6**, 376 (2010).
[12] A. Shitade, H. Katsura, J. Kuneš, X.-L. Qi, S.-C. Zhang, and N. Nagaosa, Quantum Spin Hall Effect in a Transition Metal Oxide Na_2IrO_3, Phys. Rev. Lett. **102**, 256403 (2009).
[13] F. Wang and T. Senthil, Twisted Hubbard Model for Sr_2IrO_4: Magnetism and Possible High Temperature Superconductivity, Phys. Rev. Lett. **106**, 136402 (2011).
[14] G. Cao and P. Schlottmann, The challenge of spin-orbit-tuned ground states in iridates: A key issues review, Rep. Prog. Phys. **81**, 042502 (2018).
[15] S. K. Panda, S. Bhowal, Y. Li, S. Ganguly, R. Valentí, L. Nordström, and I. Dasgupta, Electronic structure and spin-orbit driven magnetism in $d^{4.5}$ insulator $Ba_3YIr_2O_9$, Phys. Rev. B **92**, 180403 (2015).
[16] T. Dey, M. Majumder, J. C. Orain, A. Senyshyn, M. Prinz-Zwick, S. Bachus, Y. Tokiwa, F. Bert, P. Khuntia, N. Büttgen, A. A. Tsirlin, and P. Gegenwart, Persistent low-temperature spin dynamics in the mixed-valence iridate $Ba_3InIr_2O_9$, Phys. Rev. B **96**, 174411 (2017).
[17] J. S. Gardner, M. J. P. Gingras, and J. E. Greedan, Magnetic pyrochlore oxides, Rev. Mod. Phys. **82**, 53 (2010).
[18] S. V. Streltsov and D. I. Khomskii, Covalent bonds against magnetism in transition metal compounds, Proc. Natl. Acad. Sci. U.S.A. **113**, 10491 (2016).
[19] M. Ye, H.-S. Kim, J.-W. Kim, C.-J. Won, K. Haule, D. Vanderbilt, S.-W. Cheong, and G. Blumberg, Covalency-driven collapse of strong spin-orbit coupling in face-sharing iridium octahedra, Phys. Rev. B **98**, 201105 (2018).
[20] I. I. Mazin, H. O. Jeschke, K. Foyevtsova, R. Valentí, and D. I. Khomskii, Na_2IrO_3 as a Molecular Orbital Crystal, Phys. Rev. Lett. **109**, 197201 (2012).
[21] J.-i. Igarashi and T. Nagao, Analysis of resonant inelastic x-ray scattering from Sr_2IrO_4 in an itinerant-electron approach, Phys. Rev. B **90**, 064402 (2014).
[22] X. Liu, V. M. Katukuri, L. Hozoi, W.-G. Yin, M. P. M Dean, M. H. Upton, J. Kim, D. Casa, A. Said, T. Gog *et al.*, Testing the Validity of the Strong Spin-Orbit-Coupling Limit for Octahedrally Coordinated Iridate Compounds in a Model System Sr_3CuIrO_6, Phys. Rev. Lett. **109**, 157401 (2012).
[23] H. Gretarsson, J. P. Clancy, X. Liu, J. P. Hill, E. Bozin, Y. Singh, S. Manni, P. Gegenwart, J. Kim, A. H. Said, D. Casa, T. Gog, M. H. Upton, H.-S. Kim, J. Yu, V. M. Katukuri, L. Hozoi, J. van den Brink, and Y.-J. Kim, Crystal-Field

Splitting and Correlation Effect on the Electronic Structure of A_2IrO_3, Phys. Rev. Lett. **110**, 076402 (2013).
[24] J. Terzic, J. C. Wang, F. Ye, W. H. Song, S. J. Yuan, S. Aswartham, L. E. DeLong, S. V. Streltsov, D. I. Khomskii, and G. Cao, Coexisting charge and magnetic orders in the dimer-chain iridate $Ba_5AlIr_2O_{11}$, Phys. Rev. B **91**, 235147 (2015).
[25] L. J. P. Ament, M. van Veenendaal, T. P. Devereaux, J. P. Hill, and J. van den Brink, Resonant inelastic x-ray scattering studies of elementary excitations, Rev. Mod. Phys. **83**, 705 (2011).
[26] A. Föhlisch, M. Nyberg, J. Hasselström, O. Karis, L. G. M. Pettersson, and A. Nilsson, How Carbon Monoxide Adsorbs in Different Sites, Phys. Rev. Lett. **85**, 3309 (2000).
[27] M. P. M. Dean, R. S. Springell, C. Monney, K. J. Zhou, J. Pereiro, I. Božović, B. Dalla Piazza, H. M. Rønnow, E. Morenzoni, J. van den Brink *et al.*, Spin excitations in a single La_2CuO_4 layer, Nat. Mater. **11**, 850 (2012).
[28] A. Lupascu, J. P. Clancy, H. Gretarsson, Z. Nie, J. Nichols, J. Terzic, G. Cao, S. S. A. Seo, Z. Islam, M. H. Upton, Jungho Kim, D. Casa, T. Gog, A. H. Said, V. M. Katukuri, H. Stoll, L. Hozoi, J. van den Brink, and Y.-J. Kim, Tuning Magnetic Coupling in Sr_2IrO_4 Thin Films with Epitaxial Strain, Phys. Rev. Lett. **112**, 147201 (2014).
[29] M. P. M. Dean *et al.*, Ultrafast energy- and momentum-resolved dynamics of magnetic correlations in the photo-doped Mott insulator Sr_2IrO_4, Nat. Mater. **15**, 601 (2016).
[30] D. Meyers, Y. Cao, G. Fabbris, N. J. Robinson, L. Hao, C. Frederick, N. Traynor, J. Yang, J. Lin, M. H. Upton *et al.*, Magnetism in artificial Ruddlesden-Popper iridates leveraged by structural distortions, arXiv:1707.08910.
[31] M. Harland, A. I. Poteryaev, S. V. Streltsov, and A. I. Lichtenstein, Electronic correlations and competing orders in multiorbital dimers: A cluster DMFT study, Phys. Rev. B **99**, 045115 (2019).
[32] C. Gang and L. De-Long, *Frontiers of 4d- and 5d-Transition Metal Oxides* (World Scientific, Singapore, 2013).
[33] Yu V. Shvyd'ko, J. P. Hill, C. A. Burns, D. S. Coburn, B. Brajuskovic, D. Casa, K. Goetze, T. Gog, R. Khachatryan, J.-H. Kim *et al.*, MERIX: Next generation medium energy resolution inelastic X-ray scattering instrument at the APS, J. Electron Spectrosc. Relat. Phenom. **188**, 140 (2013).
[34] K. Ishii, I. Jarrige, M. Yoshida, K. Ikeuchi, J. Mizuki, K. Ohashi, T. Takayama, J. Matsuno, and H. Takagi, Momentum-resolved electronic excitations in the Mott insulator Sr_2IrO_4 studied by resonant inelastic x-ray scattering, Phys. Rev. B **83**, 115121 (2011).
[35] M. M. Sala, K. Ohgushi, A. Al-Zein, Y. Hirata, G. Monaco, and M. Krisch, $CaIrO_3$: A Spin-Orbit Mott Insulator Beyond the $j_{\mathrm{eff}} = 1/2$ Ground State, Phys. Rev. Lett. **112**, 176402 (2014).
[36] Higher resolution data were taken with 30 meV energy resolution, but this does not reveal any new features.
[37] Y. L. Wang, G. Fabbris, M. P. M. Dean, and G. Kotliar, EDRIXS: An open source toolkit for simulating spectra of resonant inelastic x-ray scattering, arXiv:1812.05735.
[38] S. Choi, P. Semon, B. Kang, A. Kutepov, and G. Kotliar, ComDMFT: a Massively Parallel Computer Package for the Electronic Structure of Correlated-Electron Systems, arXiv:1810.01679.
[39] COMSCOPE project, https://www.bnl.gov/comscope/index.php.
[40] See Supplemental Material at http://link.aps.org/supplemental/10.1103/PhysRevLett.122.106401 for details of the DFT calculations and RIXS cross section and more simulated RIXS spectra as a function of $\Delta\mu$. The Supplemental Material includes Refs. [25,41–45].
[41] P. E. Blöchl, Projector augmented-wave method, Phys. Rev. B **50**, 17953 (1994).
[42] G. Kresse and D. Joubert, From ultrasoft pseudopotentials to the projector augmented-wave method, Phys. Rev. B **59**, 1758 (1999).
[43] J. P. Perdew, K. Burke, and M. Ernzerhof, Generalized Gradient Approximation Made Simple, Phys. Rev. Lett. **77**, 3865 (1996).
[44] R. D. Cowan, *The Theory of Atomic Structure and Spectra* (University of California Press, Berkeley, 1981).
[45] Hk. Mller-Buschbaum and Ch. Lang, $Ba_5AlIr_2O_{11}$: Eine neue Verbindung mit Iridium(IV,V), Z. Anorg. Allg. Chem. **568**, 29 (1989).
[46] I. I. Mazin, S. Manni, K. Foyevtsova, H. O. Jeschke, P. Gegenwart, and R. Valentí, Origin of the insulating state in honeycomb iridates and rhodates, Phys. Rev. B **88**, 035115 (2013).
[47] Bo Yuan, J. P. Clancy, A. M. Cook, C. M. Thompson, J. Greedan, G. Cao, B. C. Jeon, T. W. Noh, M. H. Upton, D. Casa *et al.*, Determination of Hund's coupling in 5d oxides using resonant inelastic x-ray scattering, Phys. Rev. B **95**, 235114 (2017).
[48] B. J. Kim and Giniyat Khaliullin, Resonant inelastic x-ray scattering operators for t_{2g} orbital systems, Phys. Rev. B **96**, 085108 (2017).
[49] A. Paramekanti, D. J. Singh, B. Yuan, D. Casa, A. Said, Y.-J. Kim, and A. D. Christianson, Spin-orbit coupled systems in the atomic limit: Rhenates, osmates, iridates, Phys. Rev. B **97**, 235119 (2018).
[50] G. Kresse and J. Furthmüller, Efficient iterative schemes for ab initio total-energy calculations using a plane-wave basis set, Phys. Rev. B **54**, 11169 (1996).
[51] N. Marzari, A. A. Mostofi, J. R. Yates, I. Souza, and D. Vanderbilt, Maximally localized Wannier functions: Theory and applications, Rev. Mod. Phys. **84**, 1419 (2012).
[52] A. A. Mostofi, J. R. Yates, Y.-S. Lee, I. Souza, D. Vanderbilt, and N. Marzari, Wannier90: A tool for obtaining maximally-localised Wannier functions, Comput. Phys. Commun. **178**, 685 (2008).
[53] S. V. Streltsov, G. Cao, and D. I. Khomskii, Suppression of magnetism in $Ba_5AlIr_2O_{11}$: Interplay of Hund's coupling, molecular orbitals, and spin-orbit interaction, Phys. Rev. B **96**, 014434 (2017).
[54] G. Cao, J. Bolivar, S. McCall, J. E. Crow, and R. P. Guertin, Weak ferromagnetism, metal-to-nonmetal transition, and negative differential resistivity in single-crystal Sr_2IrO_4, Phys. Rev. B **57**, R11039 (1998).
[55] B. J. Kim, Hosub Jin, S. J. Moon, J.-Y. Kim, B.-G. Park, C. S. Leem, J. Yu, T. W. Noh, C. Kim, S.-J. Oh, J.-H. Park, V. Durairaj, G. Cao, and E. Rotenberg, Novel $J_{\mathrm{eff}} = 1/2$ Mott State Induced by Relativistic Spin-Orbit Coupling in Sr_2IrO_4, Phys. Rev. Lett. **101**, 076402 (2008).

[56] G. Cao, Y. Xin, C. S. Alexander, J. E. Crow, P. Schlottmann, M. K. Crawford, R. L. Harlow, and W. Marshall, Anomalous magnetic and transport behavior in the magnetic insulator $Sr_3Ir_2O_7$, Phys. Rev. B **66**, 214412 (2002).

[57] J. J. Ishikawa, E. C. T. O'Farrell, and S. Nakatsuji, Continuous transition between antiferromagnetic insulator and paramagnetic metal in the pyrochlore iridate $Eu_2Ir_2O_7$, Phys. Rev. B **85**, 245109 (2012).

[58] M. C. Shapiro, S. C. Riggs, M. B. Stone, C. R. de la Cruz, S. Chi, A. A. Podlesnyak, and I. R. Fisher, Structure and magnetic properties of the pyrochlore iridate $Y_2Ir_2O_7$, Phys. Rev. B **85**, 214434 (2012).

[59] S. M. Disseler, C. Dhital, T. C. Hogan, A. Amato, S. R. Giblin, C. de la Cruz, A. Daoud-Aladine, S. D. Wilson, and M. J. Graf, Magnetic order and the electronic ground state in the pyrochlore iridate $Nd_2Ir_2O_7$, Phys. Rev. B **85**, 174441 (2012).

[60] G. Cao, T. F. Qi, L. Li, J. Terzic, S. J. Yuan, L. E. DeLong, G. Murthy, and R. K. Kaul, Novel Magnetism of $Ir^{5+}(5d^4)$ Ions in the Double Perovskite Sr_2YIrO_6, Phys. Rev. Lett. **112**, 056402 (2014).

[61] G. Khaliullin, Excitonic Magnetism in Van Vleck–type d^4 Mott Insulators, Phys. Rev. Lett. **111**, 197201 (2013).

[62] D. Ziat, A. A. Aczel, R. Sinclair, Q. Chen, H. D. Zhou, T. J. Williams, M. B. Stone, A. Verrier, and J. A. Quilliam, Frustrated spin-$\frac{1}{2}$ molecular magnetism in the mixed-valence antiferromagnets $Ba_3MRu_2O_9$ (M = In, Y, Lu), Phys. Rev. B **95**, 184424 (2017).

[63] S. A. J. Kimber, M. S. Senn, S. Fratini, H. Wu, A. H. Hill, P. Manuel, J. P. Attfield, D. N. Argyriou, and P. F. Henry, Charge Order at the Frontier between the Molecular and Solid States in $Ba_3NaRu_2O_9$, Phys. Rev. Lett. **108**, 217205 (2012).

[64] J. P. Clancy, H. Gretarsson, E. K. H. Lee, D. Tian, J. Kim, M. H. Upton, D. Casa, T. Gog, Z. Islam, B.-G. Jeon, K. H. Kim, S. Desgreniers, Y. B. Kim, S. J. Julian, and Y.-J. Kim, X-ray scattering study of pyrochlore iridates: Crystal structure, electronic, and magnetic excitations, Phys. Rev. B **94**, 024408 (2016).

[65] C. Donnerer, M. C. Rahn, M. M. Sala, J. G. Vale, D. Pincini, J. Strempfer, M. Krisch, D. Prabhakaran, A. T. Boothroyd, and D. F. McMorrow, All-in–all-Out Magnetic Order and Propagating Spin Waves in $Sm_2Ir_2O_7$, Phys. Rev. Lett. **117**, 037201 (2016).

[66] S. H. Chun, B. Yuan, D. Casa, J. Kim, C.-Y. Kim, Z. Tian, Y. Qiu, S. Nakatsuji, and Y.-J. Kim, Magnetic Excitations across the Metal-Insulator Transition in the Pyrochlore Iridate $Eu_2Ir_2O_7$, Phys. Rev. Lett. **120**, 177203 (2018).

[67] S. Calder, J. G. Vale, N. A. Bogdanov, X. Liu, C. Donnerer, M. H. Upton, D. Casa, A. H. Said, M. D. Lumsden, Z. Zhao, J.-Q. Yan, D. Mandrus, S. Nishimoto, J. van den Brink, J. P. Hill, D. F. McMorrow, and A. D. Christianson, Spin-orbit-driven magnetic structure and excitation in the 5d pyrochlore $Cd_2Os_2O_7$, Nat. Commun. **7**, 11651 (2016).

[68] A. Revelli *et al.*, Resonant inelastic x-ray incarnation of Young's double-slit experiment, Sci. Adv. **5**, eaav4020 (2019).